

enyl-imidodiphosphate (AMP-PNP) or ATP and 10  $\mu\text{M}$  taxol at 27°C for 10 min, washed by each buffer, and processed for immunodetection (76). The vesicles on microtubules were observed in differential interference contrast laser scanning microscope (DIC-LSM). For the blocking assay, KIF17 tail peptide (GST-KIF17 939–1038) (22) was incubated with the floated vesicles for 6 hours before the microtubule binding assay. The total concentration of protein was equalized by addition of GST alone.

30. Mouse hippocampal neurons were fixed in 4% paraformaldehyde (PFA) and permeabilized with 0.1% Triton X-100 for 3 min. The brain sections were fixed in 4% PFA. For NR2B staining of the sections, pepsin treatment was performed as described (33). Anti-NR1 ( $\alpha\text{GluR}\zeta\text{1}$  No43) and NR1 mAb, anti-NR2B COOH-terminal peptide ( $\alpha\text{GluR}\epsilon$  No34), and anti-NR2B NH<sub>2</sub>-terminal peptide ( $\alpha\text{GluR}\epsilon$  No59) each gave the same results.
31. For this experiment, we first purified KIF17-bearing membrane organelles from KIF17-enriched fractions of floating assay (14). Anti-KIF17-coated beads with

vesicles attached (5  $\mu\text{l}$ ) were incubated for 1 hour in three different conditions: (i) 30  $\mu\text{l}$  of recombinant full-length KIF17 (1 mg/ml), (ii) recombinant tailless KIF17 (1–938) (1 mg/ml), and (iii) tail-deleted construct (1–938) (0.8 mg/ml) mixed with tail construct (GST-KIF17 939–1038) (0.2 mg/ml) (22). Through this process, KIF17 vesicles were detached from beads. In the third condition, tail construct was added to exclude the possible difference of detachment of the vesicles from the beads. Then, eluted supernatant was diluted in 100  $\mu\text{l}$  of motility buffer (14) and placed in the observation chamber. In all three conditions, Brownian movement of the detached vesicles was observed. In the first condition, almost all (more than 10 movements in 3 min of observation) of the vesicles that were in contact with axoneme moved. No vesicle movement on axoneme was observed in the other two conditions. Identification of vesicles correlated with motility as described (34). Of the vesicles attached to microtubules by KIF17, ~40% were NR2B<sup>+</sup>. NR2B was not detected in the vesicles isolated with anti-KIF3B immunobeads as a control.

32. M. Irie *et al.*, *Oncogene* **18**, 2811 (1999).
33. M. Watanabe *et al.*, *Eur. J. Neurosci.* **10**, 478 (1998); T. Kutsuwada *et al.*, *Neuron* **16**, 333 (1996); H. Mori *et al.*, *Neuron* **21**, 571 (1998).
34. J. Taunton *et al.*, *J. Cell Biol.* **148**, 519 (2000).
35. We thank T. Südhof for anti-mLin-10; Y. Hata for anti-mLin-7; M. Mishina for the anti-NR subunits; M. Watanabe, M. Mishina, T. Takahashi, T. Nakata, and Y. Kanai for discussions and advice; K. Yamamoto, L. Guillaud, Y. Ikeda, Y. Okada, M. Kikkawa, S. Nonaka, H. Sato, H. Fukuda, and M. Sugaya for technical assistance; and other members of the Hirokawa lab for technical assistance, stimulating discussions, and valuable advice throughout. Supported by the Japanese Society for Promotion of Science Research Fellowship for Young Scientists (T.N. and D.-H.S.) and by a Special Grant-in-Aid for Center of Excellence from the Japan Ministry of Education, Science, Sports and Culture (N.H.).

28 December 1999; accepted 17 April 2000

## REPORTS

## Forming Supramolecular Networks from Nanoscale Rods in Binary, Phase-Separating Mixtures

Gongwen Peng,<sup>1</sup> Feng Qiu,<sup>1</sup> Valeriy V. Ginzburg,<sup>1</sup> David Jasnow,<sup>2</sup> Anna C. Balazs<sup>1\*</sup>

Simulations show that when low-volume fractions of nanoscale rods are immersed in a binary, phase-separating blend, the rods self-assemble into needle-like, percolating networks. The interconnected network arises through the dynamic interplay of phase-separation between the fluids, through preferential adsorption of the minority component onto the mobile rods, and through rod-rod repulsion. Such cooperative effects provide a means of manipulating the motion of nanoscopic objects and directing their association into supramolecular structures. Increasing the rod concentration beyond the effective percolation threshold drives the system to self-assemble into a lamellar morphology, with layers of wetted rods alternating with layers of the majority-component fluid. This approach can potentially yield organic/inorganic composites that are ordered on nanometer scales and exhibit electrical or structural integrity.

Dispersion of solid nanoparticles throughout a polymer blend can dramatically improve the mechanical, thermal, or electrical properties of the mixture (1). Controlling the distribution of particles within multi-component polymeric blends, however, remains a considerable challenge. Most polymer pairs are immiscible, and thus, blends usually phase-separate. Typically, one or more of the polymers preferentially adsorb

onto the mobile particles. Thus, the motion of the particles influences the behavior of the immiscible polymeric fluids, and the structural evolution of the fluids in turn affects the dispersion of the particles (2). The situation becomes even more complex if these particles are rod-like (such as nanotubes or rigid fibers) because rods can form liquid crystalline phases (3, 4). Now, interplay among three phenomena—phase-separation, wetting, and anisotropic interparticle interactions—controls the structure of the composite.

We probed these interactions in binary fluid/rod mixtures through computer simulations and show that the irreversible evo-

lution of phase-separating fluids can be exploited to drive the self-assembly of nanoscopic rods into supramolecular networks. Applied to nanotubes, this approach could produce electrically conducting pathways in insulating materials; applied to short, inorganic fibers, the scheme could yield continuous reinforcing structures in organic/inorganic composites. Overall, the results facilitate the efficient fabrication of advanced hybrid materials.

Our two-dimensional simulation combines a coarse-grained description of the binary fluids with a discrete model for solid additives (5–9). The binary system is described by a continuous order parameter  $\psi(\mathbf{r})$ , which is the difference between the local volume fractions of components A and B,  $\psi(\mathbf{r}) = \phi_A(\mathbf{r}) - \phi_B(\mathbf{r})$ . The flux of  $\psi$  is proportional to the local gradient of the chemical potential, which in turn is proportional to the derivative of the free energy,  $F$ , with respect to the order parameter

$$\partial\psi/\partial t = \Gamma\nabla^2(\delta F\{\psi\}/\delta\psi) \quad (1)$$

where  $\Gamma$  is the order parameter mobility. The rigid rods are described by discrete entities, each of which has a center-of-mass position  $\mathbf{r}_i$  and an orientation angle  $\theta_i$ , measured from a fixed direction. The variables  $\mathbf{r}_i$  and  $\theta_i$  obey Langevin equations

$$\partial\mathbf{r}_i/\partial t = -M\partial F/\partial\mathbf{r}_i + \eta_i \quad (2)$$

$$\partial\theta_i/\partial t = -M'\partial F/\partial\theta_i + \zeta_i \quad (3)$$

where  $M$  and  $M'$  are mobility constants, and  $\eta_i$  and  $\zeta_i$  are thermal fluctuations that satisfy the fluctuation-dissipation relations. Equations 1 to 3 are discretized and numerically integrated on a 256 by 256 square lattice, which has periodic boundary conditions in both the  $x$  and  $y$  directions. The lattice sets the unit of length.

<sup>1</sup>Chemical Engineering Department and <sup>2</sup>Department of Physics and Astronomy, University of Pittsburgh, Pittsburgh, PA 15261, USA.

\*To whom correspondence should be addressed. E-mail: balazs@vms.cis.pitt.edu

The free energy that controls the evolution of the system consists of three parts:  $F = F_{GL} + F_{CPL} + F_{RR}$ , corresponding to the fluid-fluid, fluid-rod, and rod-rod interactions, respectively. The fluid is described by the Ginzburg-Landau free energy

$$F_{GL} = \int d\mathbf{r} [-a\psi^2/2 + b\psi^4/4 + c(\nabla\psi)^2/2] \quad (4)$$

where  $a$ ,  $b$ , and  $c$  are constants. The square gradient term represents the cost in free energy for creating spatial variations of the order parameter, such as interfacial regions. For the interaction between the rods and the binary mixture, we take

$$F_{CPL} = \int d\mathbf{r} \sum_i \int ds_i V(\mathbf{r} - \mathbf{s}_i) (\psi(\mathbf{r}) - \psi_w)^2 \quad (5)$$

Here,  $\mathbf{s}_i = \mathbf{r}_i + \delta\mathbf{s}_i$  represents a point on the surface of the  $i$ th particle and the constant  $\psi_w$  is set to 1 to represent preferential adsorption of species A onto the rods. The interaction  $V(\mathbf{r}) > 0$  is short-ranged, and we take  $V(\mathbf{r} - \mathbf{s}_i) = V_0 \exp(-|\mathbf{r} - \mathbf{s}_i|/r_0)$ , where  $V_0$  is a constant and  $r_0$  represents a microscopic length scale. The rod-rod interaction,  $F_{RR}$ , is taken to be purely repulsive

$$F_{RR} = \begin{cases} \chi \sum_i \sum_j (L - |\mathbf{r}_i - \mathbf{r}_j|)^2 [(4/3) - \cos^2(\theta_i - \theta_j)] & \text{for } |\mathbf{r}_i - \mathbf{r}_j| < L \\ 0 & \text{for } |\mathbf{r}_i - \mathbf{r}_j| \geq L \end{cases} \quad (6)$$

where the constant  $\chi$  characterizes the strength of the repulsion and  $L$  is the rod length (10).

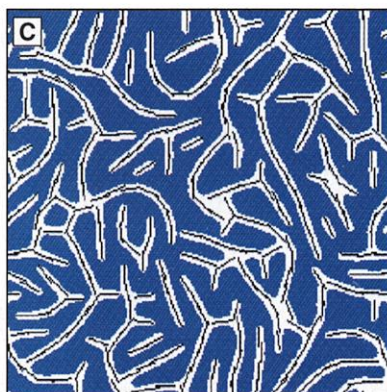
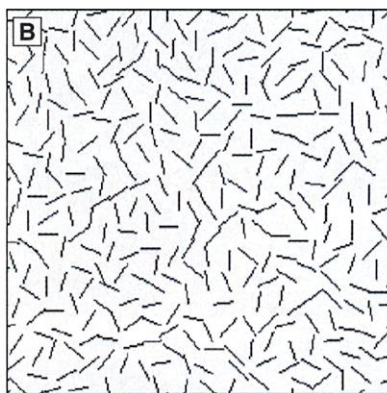
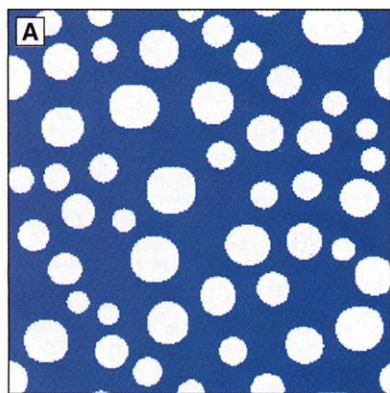


**Fig. 1.** Self-assembly of rods into a percolating network. (A) The 30:70 A/B mixture without rods. (B)  $N = 340$  rods of length  $L = 13$  (a number density of 7%) and no fluid. (C) Rods and A/B mixture after 100,000 time steps. White regions are A domains, blue regions are B domains, dark lines in the white areas depict rods. Here,  $\chi = 0.5$ , and  $\Gamma = M = M' = 1.0$ .

This interaction leads to an isotropic-nematic ordering for the pure rod system.

The rigid rods are blended with a mixture of 30% A and 70% B. An interplay between energetics (fluid-rod and rod-rod interactions) and irreversible kinetics [fluid phase-separation (5–8) and rod motion] drives the morphology of this system. The morphology of the 30:70 immiscible mixture in the absence of rods shows that the minority A phase forms isolated, spherical islands within the B matrix (Fig. 1A). In the absence of the binary mixture, the  $N = 340$  rods of length  $L = 13$  are uniformly dispersed on the lattice, and form an isotropic phase (Fig. 1B). However, when these rods are allowed to interact with the evolving blend, the system self-assembles into a supramolecular structure (Fig. 1C) that is dramatically different from Fig. 1, A or B. The rods form continuous “strings” in narrow, needle-like A domains. Both the low-volume fraction of rods and minority A component percolate, effectively connecting one edge of the material to the other (11).

Comparison of Fig. 1, B and C, reveals that the strong preferential adsorption drives the A phase to coat each rod and that the rods are strongly confined in the minority phase during the phase separation. To show that the rods are physically moved by osmotic effects resulting from the phase separation, we performed two simulations in which the rods have the same initial

configuration. In one case, the calculation is performed in the absence of the fluids [ $V(\mathbf{r} - \mathbf{s}_i) = 0$ ] and in the other case, the rods interact with the binary mixture. A comparison of the rod positions at late times (Fig. 2) shows that the temporal evolution of the fluids “pushes” and “corrals” the rods. Hence, the dynamic coupling between preferential adsorption and phase separation is critical to the formation of the network seen in Fig. 1C.

Comparison of Fig. 1, A and C, indicates that the rods effectively stretch the A droplets into elongated domains. Because of the rod-rod repulsion, the high concentrations of rods have a lower free energy when they are arranged end-to-end (beyond the range of the interaction) rather than side-by-side (Eq. 6). This end-to-end arrangement deforms the strongly wetting droplets. Hence, the rod-rod repulsion also plays a crucial role in driving the A fluid to form a percolating network.

A final simulation reveals that the mobility of the rods is critical for percolation to occur. Here,  $N = 340$  rods of length  $L = 13$  are allowed to interact for a fixed period,  $\Delta t$ , in the absence of the binary fluid. The rods are free to translate and rotate, and they form an isotropic phase, much as in Fig. 1B. At  $\Delta t = 20,000$  time steps, the position of these particles is fixed. The binary fluid is introduced into this system, and only the fluid is allowed to evolve with time. After an additional 20,000 steps, an A-rich layer is seen to coat the fixed rods, but neither the rods nor the fluid percolates. When the rods are allowed to move and the simulation is run for another 20,000 steps, the coated rods form a distinct needle-like network that extends from one side of the lattice to the other.

The observed transition between the droplet and needle-like network can be an-

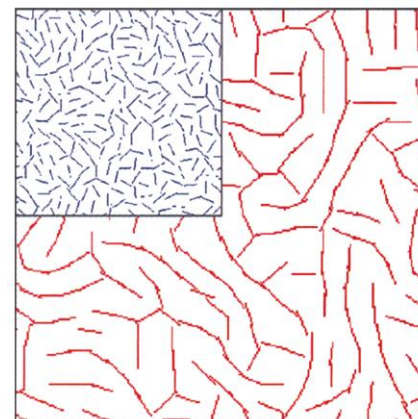


**Fig. 2.** Rod positions in the presence and absence (inset) of the binary fluids. Rod length and number as in Fig. 1. The fluid “corrals” rods into percolating pathways.

alyzed through the following qualitative argument. Consider an A-phase droplet that contains  $N$  rods. The energy of the droplet has the form

$$F = A \log(N) + BN^{1/2} + CN + \text{const.} \quad (7)$$

where the constants  $A$ ,  $B$ , and  $C$  depend on the droplet anisotropy and details of the repulsive rod-rod potential. The third term is the bulk energy for rods within the droplet. The second term arises from two contributions: (i) the interfacial free energy per unit area,  $\sigma_{AB}$  (the surface tension), associated with immiscible fluids and (ii) the energy gain due to rods near the interface (because these rods interact with fewer of their neighbors than rods in the bulk). The first term describes the energy of a point-like orientational defect (3), arising from the fact that rods prefer to lie parallel to the interface. Mean-field estimates for  $A$ ,  $B$ , and  $C$  that correspond to the simulations are

$$A = (\chi/6)L^2 [1 - (1/q_1 \rho f_A L^2)] \alpha \quad (8)$$

$$B = (\sigma_{AB} \alpha^{-1/2} + [\sigma_{AB} - (\chi/q_2)L \{1 - (1/q_1 \rho f_A L^2)\}^2] \alpha^{1/2}) (\pi \rho f_A)^{-1/2} \quad (9)$$

$$C = (\chi/3)L^2 [1 - (1/q_1 \rho f_A L^2)]^2 \quad (10)$$

where  $\alpha = R_x/R_y$  is the droplet aspect ratio ( $R_{j=x,y}$  is the typical droplet size in the  $j$  direction),  $\rho$  is the rod number density,  $f_A$  is the volume fraction of A, and  $q_1$  and  $q_2$  are constants on the order of unity. In the thermodynamic limit ( $N \rightarrow \infty$ ), the shape of the droplet is determined by the surface term  $B$  (Eq. 9) (the bulk term,  $CN$ , is independent of  $\alpha$ ). Minimization of  $B$  with respect to  $\alpha$  shows that the system exhibits two different types of behavior depending on the rod density (given a sufficiently large rod length,  $L$ , and interaction strength,  $\chi$ ). The transition density,  $\rho^*$ , is

$$\rho^* = (q_1 f_A L^2)^{-1} [1 - (q_2 \sigma_{AB} / \chi L)^{1/2}]^{-1} \quad (11)$$

If  $\rho \leq \rho^*$ , both terms on the right-hand side of Eq. 9 are positive, and the droplet has a finite aspect ratio even when  $N \rightarrow \infty$ . This situation corresponds to a droplet morphology. For  $\rho > \rho^*$ , the second term on the right-hand side is negative, and the surface energy is minimized when  $\alpha \rightarrow \infty$ . The defect term (proportional to  $\ln N$ ) in Eq. 7 cuts off the unbounded growth of  $\alpha$ , and we obtain  $\alpha$  on the order of  $N$ . This corresponds to the “droplet” having a constant width ( $R_y$ ) and length  $R_x \sim N$ , which corresponds to our percolating needle morphology. Equation 11 indicates that the onset of network formation can be controlled by varying  $\chi$ ,  $\sigma_{AB}$ , or  $L$  (12).

Through the simulation, we can estimate  $\rho^*$ , the density of rods that are needed to effectively form a percolating network, for different  $L$  (Fig. 3). The data are consistent with the  $L$  dependence predicted in Eq. 11. Also plotted (Fig. 3) are the percolation thresholds for the pure rod systems, in the absence of the binary fluid. What is striking is that for most cases, the numbers differ by roughly a factor of 2. Thus, significantly fewer repelling nanotubes would be required to form a network if these rods are blended in such a binary mixture than if they were added to a single-component ma-

trix. The number of rods needed for percolation can be suppressed even below the values in Fig. 3 by decreasing the volume fraction of the minority phase.

For  $\rho > \rho^*$ , there exists a range of number densities for which the system self-assembles into the microstructure seen in Fig. 4. The A-coated rods form alternating layers with the elongated B domains, and the pattern resembles the morphology of microphase-separated diblock copolymers. This structure does not appear to coarsen further with time, and the width of the B domains is on the order of the interparticle distance. The rod-reinforced A regions will display greater strength than the soft B domains, and the uniformly dispersed rods can improve the mechanical behavior of the entire matrix. If, however, the number density is increased significantly beyond  $\rho^*$ , this lamellar morphology is destroyed. Now, there are too many rods to be accommodated in the A region and the rods are forced into the B matrix.

Our results indicate that the behavior of phase-separating fluids containing interacting, solid particles can be exploited to create a rich diversity of new structures and useful nanocomposites (13). In designing these hybrid materials, our simulations provide an efficient method for determining how variations in the characteristics of the components affect the temporal evolution of the mixture, dispersion of the particles, and homogeneity of the hybrid.

#### References and Notes

1. A. Karim *et al.*, *Macromolecules* **32**, 5917 (1999), and references therein.
2. H. Tanaka, A. J. Lovinger, D. D. Davis, *Phys. Rev. Lett.* **72**, 2581 (1994).
3. P. G. de Gennes and J. Prost, *Physics of Liquid Crystals* (Oxford Univ. Press, Oxford, ed. 2, 1993), chap. 4.
4. M. Adams *et al.*, *Nature* **393**, 349 (1998), and references therein.
5. V. V. Ginzburg *et al.*, *Phys. Rev. Lett.* **82**, 4026 (1999).
6. V. V. Ginzburg *et al.*, *Phys. Rev. E* **60**, 4352 (1999).
7. F. Qiu *et al.*, *Langmuir* **15**, 4952 (1999).
8. A. C. Balazs *et al.*, *J. Phys. Chem. B* **104**, 3411 (2000).
9. The method is similar to the one used by Kawakatsu *et al.* (14) to describe ternary oil/water/surfactant mixtures. In our system, however, the additives are rigid rods that localize in one of the phases, rather than surfactants that bind to the interfaces.
10. Coating the rods with A-type chains provides a mechanism for simultaneously obtaining steric repulsion between the rods and the preferential wetting.
11. In binary mixtures of liquid crystals and flexible coils, a minority coil phase can temporarily form a network; however, this network evolves into droplets within a relatively short time (15).
12. Droplets form if  $(\chi L / q_2 \sigma_{AB}) < 1$  according to the mean-field analysis.
13. We are extending the simulation to capture the structures that are formed in three dimensions.
14. T. Kawakatsu *et al.*, *J. Phys. Condens. Matter* **6**, 6385 (1994).
15. A. M. Lapena *et al.*, *Phys. Rev. E* **60**, R29 (1999).
16. This work was supported by grants from the Army Research Office, NSF, U.S. Department of Energy, and the Office of Naval Research.

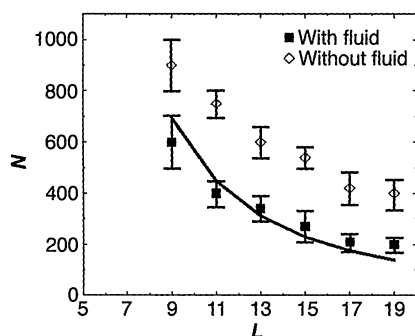


**Fig. 3.** Percolation threshold for the rods with (squares) and without (circles) the A/B fluid mixture as a function of rod length. The solid line represents the best fit according to Eq. 11 with  $q_1 = 5.5$  and  $q_2 = 0.5$ .

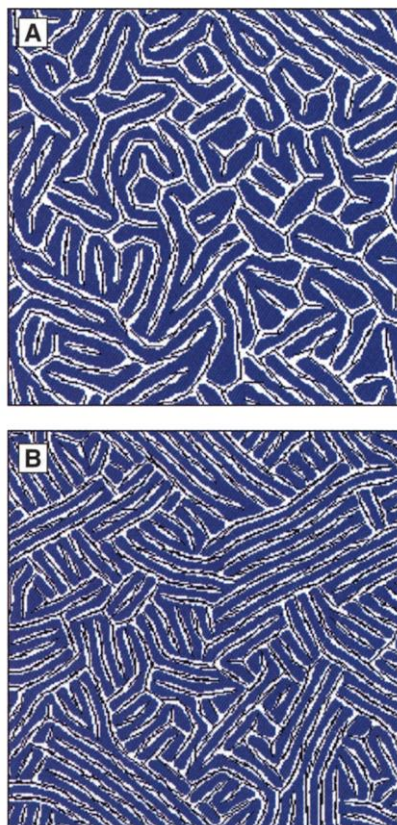


**Fig. 4.** Representative lamellar morphologies. (A)  $N = 600$ ,  $L = 13$ ; (B)  $N = 1000$ ,  $L = 11$ .

15 February 2000; accepted 27 April 2000